ELSEVIER

Seminars in
NUCLEAR
MEDICINE

Novel Quantitative PET Techniques for Clinical Decision Support in Oncology

Habib Zaidi,[*,†,‡,§] Abass Alavi,[‖] and Issam El Naqa[¶]

Quantitative image analysis has deep roots in the usage of positron emission tomography (PET) in clinical and research settings to address a wide variety of diseases. It has been extensively employed to assess molecular and physiological biomarkers in vivo in healthy and disease states, in oncology, cardiology, neurology, and psychiatry. Quantitative PET allows relating the time-varying activity concentration in tissues/organs of interest and the basic functional parameters governing the biological processes being studied. Yet, quantitative PET is challenged by a number of degrading physical factors related to the physics of PET imaging, the limitations of the instrumentation used, and the physiological status of the patient. Moreover, there is no consensus on the most reliable and robust image-derived PET metric(s) that can be used with confidence in clinical oncology owing to the discrepancies between the conclusions reported in the literature. There is also increasing interest in the use of artificial intelligence based techniques, particularly machine learning and deep learning techniques in a variety of applications to extract quantitative features (radiomics) from PET including image segmentation and outcome prediction in clinical oncology. These novel techniques are revolutionizing clinical practice and are now offering unique capabilities to the clinical molecular imaging community and biomedical researchers at large. In this report, we summarize recent developments and future tendencies in quantitative PET imaging and present example applications in clinical decision support to illustrate its potential in the context of clinical oncology.
Semin Nucl Med 48:548-564

Introduction

Positron emission tomography (PET) imaging offers the unique ability to image, with pertinently high sensitivity and specificity, the physiological or pathologic progress of many major biochemical processes underlying normal and tumor tissues. Indeed, a significant portion of the clinical value of oncologic PET stems from its inherent capability to measure individual counts that ultimately form, at the end of each acquisition, a 3D image signal directly related to the actual quantity of the true source signal, that is, the actual tracer distribution at the moment of acquisition.[1] Thus, its clinical relevance reclines in its natural aptitude to provide robust and reproducible quantitative estimates of biological or physiological processes pertinent in diagnosis, staging, therapy monitoring or treatment planning in clinical oncology. Therefore, maintaining a high quantification level in clinical PET images is very important and ensures the rest of PET benefits are efficiently exploited. Therefore, modern clinical PET scanners, in the form of hybrid PET/CT or PET/MRI systems, are equipped with advanced hardware and software systems to allow for the meticulous measurement and modeling of a wide spectrum of PET resolution degradation factors in order to later compensate as accurately as possible for their impact in PET signal quantification.

*Division of Nuclear Medicine and Molecular Imaging, Geneva University Hospital, Geneva, Switzerland.
†Geneva Neuroscience Centre, University of Geneva, Geneva, Switzerland.
‡Department of Nuclear Medicine and Molecular Imaging, University of Groningen, Groningen, the Netherlands.
§Department of Nuclear Medicine, University of Southern Denmark, Odense, Denmark.
‖Department of Radiology, Hospital of the University of Pennsylvania, Philadelphia, PA.
¶Department of Radiation Oncology, University of Michigan, Ann Arbor, MI.
Address reprint requests to Habib Zaidi, PhD, Division of Nuclear Medicine and Molecular Imaging, Geneva University Hospital, 1211 Geneva, Switzerland. E-mail: habib.zaidi@hcuge.ch

 https://doi.org/10.1053/j.semnuclmed.2018.07.003
0001-2998/

Hybrid PET/CT imaging instrumentation has emerged as a molecular imaging technology enabling concurrent morphologic and molecular characterization of tissues. The literature is populated with a large number studies proving the clinical role of hybrid imaging especially for oncologic applications. Although more recent PET/MRI technology is still considered to be in an embryonic state, its clinical role is being defined and established considering cost/benefit aspects.

Progress and innovative development of novel tracers targeting various aspects of tumor biology, including metabolism, cell proliferation, cell death, oncogene expression, drug delivery, and tumor hypoxia, are enhancing the differentiation of malignant lesions from normal tissues. The list of novel molecular imaging probes having the potential for clinical routine use in the coming years is very long.[2,3] A number of these novel tracers are expected to play a significant role in clinical diagnosis and to guide treatment decisions and therapy planning.[4,5] However, the choice of specific tracers or their combination, when the imaging should be performed during the course of therapy, and how the optimal imaging protocol should be selected and combined with robust and relevant image-derived PET metrics for assessment of disease are still open research questions offering many opportunities for future research.

Quantitative PET imaging has nowadays become an important component in the management of oncological patients. In clinical oncology, quantitative PET has turned out to be a prevailing procedure in the majority of academic clinical centers worldwide and is commonly implemented in protocols adopted in clinical trials. Accurate PET quantification is witnessed to be a key breakthrough enabling to unlock new avenues for diagnosis, monitoring of treatment response, and therapy planning. Quantitative PET imaging is expected to produce a paradigm shift and will assist in charting personalized treatment strategies and also in prospecting novel therapeutic opportunities. Previously, the foundations and limitations of quantitative PET imaging have been described in dedicated textbooks[6] and a number of review papers.[7-14] In this review, we focus on recent developments. This review describes technical advancements in the field focusing on recent advances in quantitative PET imaging and related image processing issues with special emphasis on its applications in the context of clinical oncology.

Quantitative PET Analysis

PET data acquisition protocols used in the clinic most often involves scanning at a single time window. Furthermore, depending on the scanner's axial field-of-view (FOV), clinical PET protocols may include a single or multiple bed positions, or simply beds, to cover the targeted FOV of a study. The bed frames should ideally correspond to a postinjection time point, for which the activity uptake and contrast are expected to be sufficient for the targeted region and the selected tracer relative to the surrounding background tissues. The acquired PET raw data, in units of coincidence counts per milliliter (counts/ml), are integrated at each line of response (LOR) position along the scan time window or frame of the respective bed. Then, the LOR data are normalized by the duration of the bed frame, in units of seconds, and scaled by the inverse of the nominal scanner sensitivity, in units of cps/Bq to estimate the raw detected activity concentration at each LOR of that bed position, in units of Bq/ml.

The temporally listed raw coincidence counts, also known as list-mode data, corresponding to a particular time frame are first binned or histogrammed to their respective LOR bins to ultimately form a single 3D sinogram or histogram for that time frame. Later, the produced sinogram can be reconstructed with a histogram-based 3D algorithm, on an LOR bin-by-bin basis, to estimate the respective 3D spatial distribution of the estimated average activity concentration over the time frame. Alternatively, the PET activity concentration image can be directly estimated from the list-mode PET data, on an event-by-event basis, via a list-mode 3D PET reconstruction algorithm.[15]

Regardless of the whether the reconstruction is performed in sinogram space or directly from the list-mode file, static PET images for each bed position are produced representing the 3D spatial distribution of the radioactivity concentration in vivo of the tracer (in Bq/ml). In an effort to standardize the quantitative assessment and simplify the comparison of whole-body (WB) PET images produced by different protocols on various commercial PET scanners, the concept of standardized uptake value (SUV), obtained by dividing the decay-corrected activity concentration in a malignant lesion by the patient's weight (in kg) and administered activity (in MBq), was established.[16] Depending on the volumetric characteristics and regional properties of the defined region of interest (ROI), first-order histogram metrics such as the mean, maximum, or peak SUV values can be estimated. Additional quantitative metrics including the tumor-to-background ratio (TBR) or contrast and the contrast-to-noise ratio (CNR) may also be assessed by defining ROIs in the target and background. However, the commonly employed semiquantitative metric of SUV is subject to large variability and does not capture local heterogeneity in the PET uptake, owing to its dependence on ^{18}F-FDG blood concentration and tissue kinetics.

Indeed, the activity concentration in living tissues changes dynamically with postinjection time, as regulated by the in-vivo physiological tissue uptake of the administered radiotracer.[17] As a result, the PET images estimated from 3D static data may only approximate the average 3D activity concentration distribution of the tracer over a single acquisition time frame at each bed position. Thus, static PET data and respective images produced from relatively long time frames or during fast tracer kinetics may be less representative of the tracer activity concentration at any given time moment during the acquisition, thereby of limited quantitative value.

Therefore, static clinical PET scan protocols are optimally designed for each tracer and scanner, such that they involve bed frames of the shortest possible duration, to shorten total scan duration and patient motion probability, thus retaining quantitative accuracy, while not diminishing count statistics,

thereby quantitative precision, for a given scanner sensitivity. Moreover, the acquisition time post injection should be chosen such that the tracer uptake and contrast expected in the targeted regions are high enough compared to background and sufficiently stable to guarantee adequate noise-equivalent count statistics and minimum temporal count variance in the acquired data. As a result, an important set of following parameters should be considered for the determination of the average activity concentration levels expected in a particular bed and time frame when optimizing static PET imaging protocols[14]: (i) the tracer decay rate, (ii) the nominal sensitivity of the PET scanner, and (iii) the tracer kinetics for the targeted clinical cases. The latter parameter depends on a wide range of normal and tumor physiological factors, thereby requiring dynamic PET scans to acquire the necessary data for the establishment of a reliable kinetic model.

Dynamic imaging in connection with mathematical compartmental modeling portraying the behavior of tracers in various cells was developed, thereby providing insights into various components of physiological parameters in vivo. Parametric WB PET imaging was recently introduced and is now receiving considerable attention.[18] In this regard, significant progress was also achieved in the area of 4D PET reconstruction, thus enabling to directly estimate kinetic parameters from the measured data through appropriate modeling of uncorrelated Poisson noise distribution in the PET data.[19,20] With improvements using direct 4D reconstruction methods over the traditional postreconstruction analysis often depending on the noise level and with microparameters being noisier than macroparameters, direct 4D reconstruction methods could potentially deliver significantly improved microparametric maps in the body, which could offer additional clinical information compared to current macroparametric maps.[21]

Limitations of Quantitative PET Imaging

The challenges faced by quantitative PET/CT imaging have been investigated since the commercial introduction of this technology in 2001, and a large number of professional societies established committees and task groups (eg Quantitative Imaging Biomarkers Alliance (QIBA) by RSNA, Centers of Quantitative Imaging Excellence (CQIE) by the ACRIN, Quantitative Imaging Network (QIN), AAPM Task Group 145, etc) have been established to support and promote the use of quantitative imaging biomarkers in the context of cancer screening, prediction, and assessment of response to treatment.[22,23] This is a very hot topic, which is expected to nurture as highly specific targeted molecular imaging probes are conceived and approved in diverse clinical applications including oncology. Research in the area of quantitative imaging is well underway, and the remaining technical challenges in this area are likely to be resolved within the next decade.

The deployment of hybrid PET/MRI in the clinic poses new challenges and additional difficulties, which are still open research questions and, as such, advanced algorithms enabling quantitative imaging biomarkers using this technology have to be developed and validated. Quantitative PET/MRI is still challenged by the lack of reliable and robust attenuation and motion correction methodologies enabling to produce artifact-free and quantitative PET images, with robust and reliable quantitative indices for routine application and advanced tools for multiparametric imaging for research applications.

Limitation 1: Low Sensitivity of PET

The limited sensitivity of PET scanners is one of the main physical factors impacting the accuracy of PET quantification. Substantial progress has been achieved during the last decade in PET detector technology, particularly the advent of solid-state photodetectors, such as silicon photomultipliers, which enable the implementation of time-of-flight (TOF) capability also on hybrid PET/MRI systems. When exploiting TOF information, the spatial location of annihilation photons is restrained to a segment along each LOR, which enables to reduce the cross-dependencies of image voxels, thus improving the signal-to-noise ratio and convergence rate. The exploitation of TOF information enables to reduce statistical noise in the data and as such, TOF acts as sensitivity booster.[24] Using a PET scanner equipped with TOF capability is certainly a bonus and enables the implementation of sophisticated techniques for handling image correction problems.

Artifacts may also occur due to the nonuniform detection efficiencies across the projection data space because of geometry, detector efficiency, and electronic factors, each defining a respective component that can be measured and later modeled within the calculated normalization correction factors.[25] Normalization correction factors can then be applied during reconstruction. These effects are usually well taken care of on commercial PET scanners.

Stationary multibed acquisitions adopted for WB PET scanning in the clinic, owing to the limited axial FOV of PET scanners, are commonly performed through step-wise translation of the table across the body region to be covered (usually from head to toe). This scanning mode is referred to as step-and-shoot (SS) acquisition is implemented on virtually all commercial PET/CT scanners owing to its simplicity. A major drawback of this approach is the nonuniform sensitivity across the axial FOV for fully 3D acquisition mode. Indeed, the oblique LORs contribute to the enhanced coverage of the central section of the PET scanner's axial FOV, which consequently results in higher sensitivity in this section. The net effect is the low sensitivity at the two edges of each bed position, resulting in higher statistical noise. FOVs in the axial edges of each bed are going to be propagated to the respective edges of the PET images during reconstruction. Inevitably, the simple addition on the image space of the noisy edge transaxial slices of the PET images at the overlapped regions is not expected to fully recover their degraded statistical quality triggered by the low-count reconstruction in the bed edges. Accordingly, quantification of malignant

lesions located in the overlapped regions may be disturbed in SS-PET scans, due to the enhanced noise or noise-induced bias, if the count statistics are not sufficient in the overlapped edges of both bed FOVs. This may be a serious source of quantitative errors in clinical oncologic PET studies, as many current scan protocols involve multibed SS acquisitions with gradually shorter scan times per bed.

An alternative acquisition mode, referred to as continuous bed motion, consists in a smooth translation of the scanner's bed to circumvent the above-discussed limitation of SS multibed PET scanning.[26] The aim is to render the axial sensitivity profile uniform by scanning all slices of the patient's body at a constant bed speed, excluding the two edges of the axial FOV corresponding to the start and end positions of the moving bed. Modulation of the bed speed for patient-specific WB scanning aims at maximizing the counting statistics in the ROI.[27] This feature may be utilized to focus on the region containing the pathology if known a priori.

Limitation 2: Imperfect Image Reconstruction

Despite the progress in image reconstruction from iterative statistical algorithms, enabling more accurate modeling of the data acquisition process and statistical noise, to TOF and resolution-recovery image reconstruction enabling to achieve uniform resolution throughout the FOV, image reconstruction still remains imperfect, thus impacting the quantitative accuracy of PET images. In clinical settings, the iterative process is often terminated prior to reaching convergence to produce good quality images suitable for visual interpretation. This might jeopardize quantitative accuracy, and as such, task-based image reconstruction should be considered since incompletely converged EM images are more suitable for lesion detection purposes, whereas fully converged EM images are more appropriate for quantitative analysis and estimation of physiologically meaningful parameters.[28]

Limitation 3: Photon Attenuation and Compton Scattering

The attenuation of annihilation photons in biological tissues is considered as the one of the most important physical degrading factors affecting PET image quality and quantitative accuracy. Photon attenuation results from the combined effect of Compton scattering and photoelectric absorption, the latter being almost negligible for 511 keV photons in biological tissues. In essence, Compton scattering is the companion of photon attenuation in the sense that a significant portion of attenuated photons can potentially be detected as a scattered event. Both physical degrading factors are well dealt with using end-user software implemented on commercial PET/CT scanners, although PET images generated on these systems might present artifacts and quantitative bias in the presence of metallic artifacts[29] or contrast medium.[30]

The problem of photon attenuation is more complex to solve on hybrid PET/MRI systems since contrary to x-ray CT, which inherently provides information about the electron density and, thus, the linear attenuation coefficient at each pixel in the patient's CT image, MRI provides information about proton density and relaxation time properties of biological tissues. As such, there is no direct relationship between MRI intensities and linear attenuation coefficients to build a patient-specific attenuation map. The challenges of MRI-guided attenuation correction in WB PET/MRI were addressed through the emergence of mainly three categories of approaches listed as follows: (i) segmentation-based approaches, which segment MR images into different tissue classes and assign predefined attenuation coefficients to each class, (ii) atlas-based and machine learning (ML) techniques in which co-registered MR-CT atlas pairs are used to derive a pseudo-CT image or to learn a mapping function that predicts the pseudo-CT from actual patient's MRI, and (iii) the recently revisited joint emission and attenuation reconstruction algorithms or maximum likelihood reconstruction of attenuation and activity (MLAA), in which the attenuation map is estimated from emission or transmission data.[31] Figure 1 shows a representative clinical FDG brain PET study comparing various attenuation correction strategies.

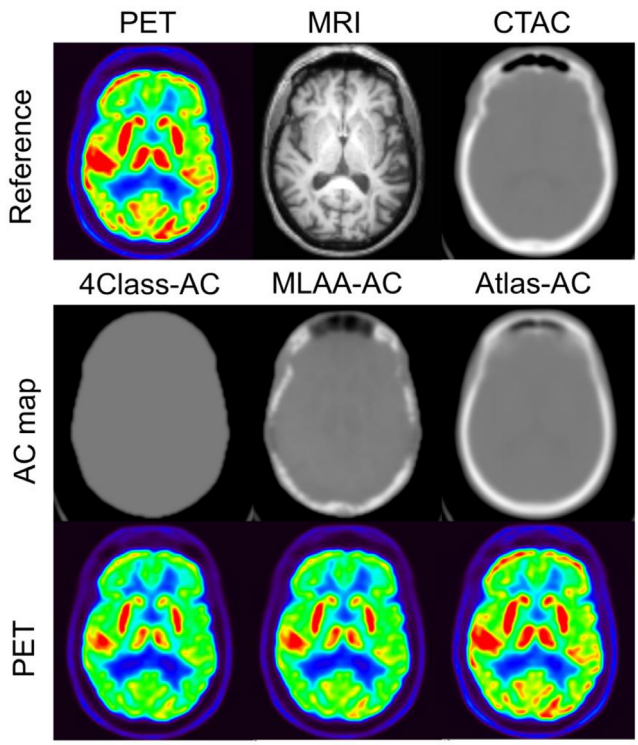

Figure 1 Representative clinical FDG brain PET study showing from left to right. (Top row) PET, MR, and CT images used as reference for evaluation. (Middle row) Attenuation maps derived using different attenuation correction approaches including segmented MRI, atlas-based, and MLAA techniques. (Bottom row) Corresponding reconstructed PET images. Note the limitations of segmented MRI-based approach that ignore the skull and air cavities. The Atlas-based approach better matches the patient's CT image, clearly outperforming the MLAA algorithm.

Limitation 4: Partial Volume Effect

Partial volume effect (PVE) is caused by the limited spatial resolution of the PET scanner and has resulted in suboptimal visualization and quantification of objects imaged. PVE leads to small abnormalities appearing larger in size but lower in signal intensity, as a result of spillover effect from the actual source to the surrounding background. This effect becomes more pronounced in lesions that are subject to respiratory and cardiac motions. The ultimate achievable spatial resolution for current WB PET scanners is 4-5 mm measured using current standards for assessment of performance characteristics (point sources), but the realistic values in human studies are substantially lower and in the range of 8-10 mm. We should point out that also the contrast resolution decreases with the decrease of lesion size. As such, it is not possible to quantify tracer concentrations accurately in lesions smaller than approximately 2-3 times the PET's spatial resolution represented by the full width at half-maximum of the scanner's point spread function. Therefore, PVE results in significant underestimation of true tracer concentration and unavoidably, partial volume correction (PVC) must be employed for accurate quantification of the data generated. Recovery coefficients are commonly calculated by scanning hot spheres with known diameters positioned within a cylindrical phantom containing low background activity. The recovery coefficients are calculated using SUV_{max} in the spheres and background SUV_{mean}, and these values can be used to correct for PVE. The recovery correction vs sphere diameter revealed a typical logarithmic curve.[32] These measurements were made by using an Allegro PET scanner (Philips Medical Systems, Best, the Netherlands).[33]

Several strategies have been proposed to overcome and correct for PVE,[34] but their review falls outside of the scope of this scientific communication. However, the consequence of PVC cannot be underestimated in both clinical and research studies. In recent years, some software packages have been introduced that allow for practical and accurate PVC.[35] In patients with lung cancer, PVC has been shown to increase SUV measurements from 55% to 89% in lesions less than 2 cm in size.[36] In breast cancer, partial volume and blood glucose level corrected SUVs resulted in the uppermost diagnostic accuracy among a range of image-derived PET metrics.[37] In brain PET imaging, anatomically (MRI) guided voxel-based PVE correction has been adopted as a sensitive approach in research settings in a number of institutions. Figure 2 illustrates transverse views of an FDG-PET image of a patient with probable Alzheimer's disease (AD).[38]

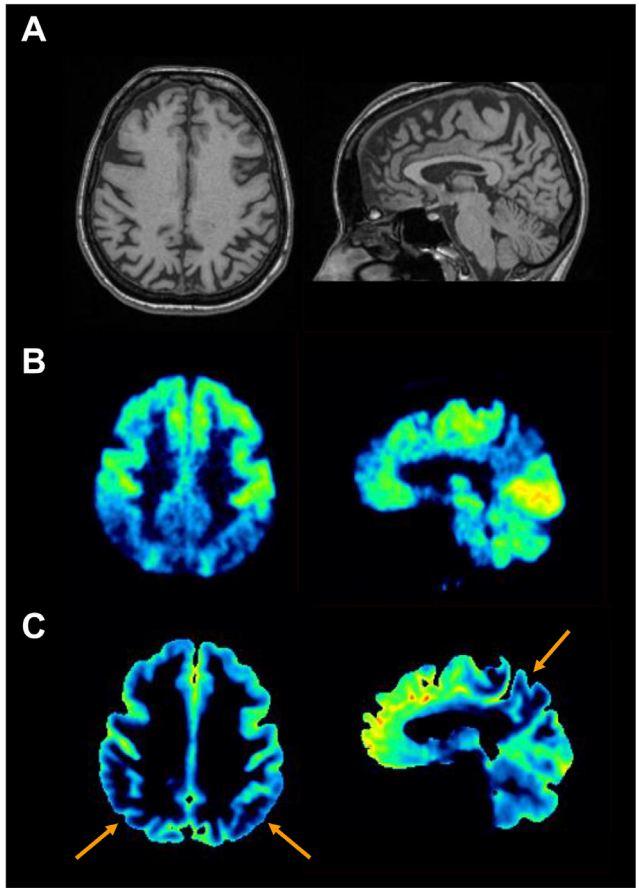

Figure 2 Illustration of MRI-guided PVC impact in functional brain PET imaging showing for a patient with probable AD. The original T1-weighted MRI (A) and PET image before (B), and after partial volume effect correction (C). The arrows put in evidence that the hypometabolism extends beyond the atrophy. Reprinted with permission from Zaidi et al.[38]

Limitation 5: Physiological and Bulk Motion

Respiratory motion is a major factor in accurate measurement of tracer concentration on PET images, and its effect is more prominent in abnormalities that are located in the lower thorax or in the upper abdomen. The misalignment between PET and CT images owing to respiratory or bulk motion has been shown to be very challenging, and none of the approaches proposed appear to address this very serious issue at this time.[39,40]

Current clinical CT systems are capable of scanning with a high speed (100 cm in the craniocaudal axis in 20 s) and generate images with a high resolution. Conversely, PET data acquisition lasts 2-5 min per bed position during multiple cardiopulmonary cycles. The difference in terms of temporal resolution between PET and CT results in different breathing patterns that also contribute to misregistration of lesions, thus leading to compromised and inaccurate quantification.[6] Therefore, either respiratory or cardiac motions result in degrading the quality of the images acquired.

Respiratory gating has been proposed to resolve the problem of misalignment by reducing the impact of motion artifacts. Unfortunately, the application of 4D PET has been of limited value in overcoming these challenges due to the relatively long total acquisition time. Furthermore, it has been difficult for patients to keep their arms over their head for an extended period of time, and this has compromised PET data acquisition. Issues related to physiological motion become even more complicated when attempts are made to image cardiac disorders (coronary atherosclerosis).

Standard Quantitative Metrics

Static Metrics (SUV, TLG, MTV, etc)

The SUV, representing the amount of tracer uptake in a malignant lesion at a discrete time post injection, is the most commonly used semi-quantitative metric used in clinical oncology owing. This quantity is usually normalized to the injected activity and patient's weight characterizing the whole body distribution volume.[16] There are a number of variants to SUV, including the maximum SUV (SUV_{max}), representing the pixel having the highest SUV, the mean SUV (SUV_{mean}), representing the average SUV in all voxels within a delineated volume of interest (VOI), and the peak SUV (SUV_{peak}), representing mean SUV in a spherical VOI having a diameter of 1.2 cm (volume of 1 cc).[41] Figure 3 shows the principles and mathematical equations used to measure these variants of the SUV metric. SUV_{mean} is more susceptible to PVE-induced errors and is also sensitive to the way the lesion contour is delineated. Overall, SUV_{max} is commonly used in the clinic owing to its simplicity and convenience whereas the SUV_{peak} has been advocated as a more relevant metric, less vulnerable to techniques used for tumor delimitation and to statistical noise typically present in PET images.[41]

A number of studies have reported that it is more appropriate to normalize the SUV with other quantities, such as lean body mass (SUV_{LBM} or SUL)[42] and body surface area (SUV_{BSA})[43] to consider that adipose tissue is not as metabolically active as other tissues. Moreover, contrary to SUV normalized to body weight, SUL is deemed to be more stable among patients and less prone to variability.[41] SUV measurements are highly reproducible[44] and are implemented on virtually all commercial and open-source multimodality medical image visualization and analysis software platforms used in clinical environments. It is worth noting that caution is required as substantial variability was observed among the various platforms, which might have consequences on multicentre clinical trials involving quantitative analysis of PET images.[45]

The metabolically active tumor volume is another image-derived PET metric reported to have prognostic value and is often used in the assessment of response to treatment. Manual delineation of the metabolically active tumor volume is the de facto standard performed in the clinic. However, the approach is challenged by the lack of clear edges between malignant lesions and normal tissues, which complicates the extraction of malignant lesions from noisy PET images. In addition, this technique is prone to errors, is operator-dependent, and suffers from intra- and inter-variability. A number of semi-automated and fully automated PET image segmentation techniques with various degrees of success have been described in the literature.[46] So far, very few of them have been adopted for use in the clinic owing to the lack of guidelines on which method should be used and the lack of confidence in those metrics in the absence of convincing evaluation and validation studies.

In essence, the AAPM's Task Group 211 report[47] recommends the use of various types of data to validate PET image segmentation strategies, including simulated, experimental phantom, and clinical studies. Clinical images lacking ground-truth with only a surrogate provided by manual delineation are commonly used to evaluate/validate segmentation algorithms, which is insufficient. The AAPM Task Group 211 report also recommends the combined use of sensitivity and positive predictive value to evaluate the accuracy of segmentation algorithms with respect to the ground-truth, since Dice coefficients are known to be sensitive to the size of the tumor and as such do not give the full picture in terms of false-positive and false-negative results.[48] More recently, the MICCAI challenge on PET segmentation[49] demonstrated that deep learning convolutional neural network (CNN) approaches achieved the best performance and do not require large datasets for training (provided data augmentation is used).

Alavi et al. were the first to introduce the concept of global assessment of metabolism in 1993 for assessment of patients with AD compared with age-matched controls.[50] The technique involved multiplying the segmented brain volumes measured by MRI by the mean cerebral metabolic rate of glucose as measured by FDG-PET and demonstrated significant differences between the two groups. The concept introduced the necessity of combining volumetric and metabolic data into one measurement to reflect global disease burden. In a report from 1999, this approach was adopted to measure total lesion glycolysis (TLG) to calculate global disease

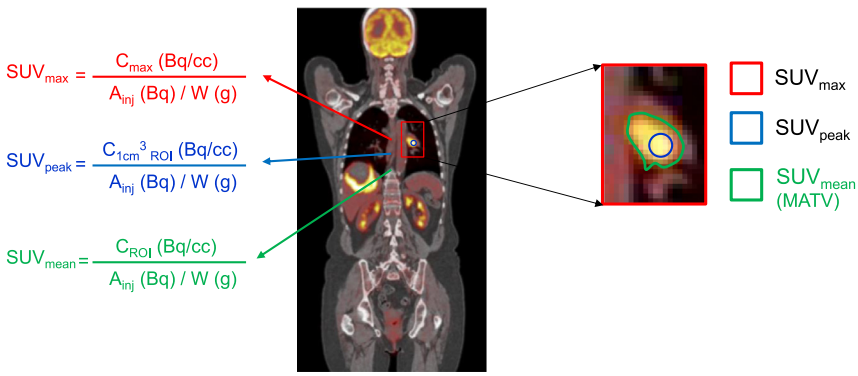

Figure 3 Illustration of the basic foundations of PET quantification and the factors involved in the calculation of first- and second-order image-derived PET metrics used in clinical oncology.

activity in cancer.[51] It was shown that TLG is strongly correlated with other PET response parameters and is reproducible. Therefore, it was concluded TLG provides complementary information to conventional SUV and its variants that are important in cancer patients.

With the advances made in medical image segmentation and delimitation of tissues over the years, global disease assessment has become a reality. This methodology has been effectively employed in quantifying malignant mesothelioma,[52] lymphoma,[53] sarcoidosis,[54] Crohn's disease,[55] radiation pneumonitis,[56] osteoarthritis,[57] rheumatoid arthritis,[58] and atherosclerosis.[59-61] Existing commercial software available today allows segmentation that generates the metabolically active tumor volume and the partial volume corrected SUV_{mean} ($pvcSUV_{mean}$). Thereafter, partial volume corrected metabolic volume product (pvcMVP) can be measured as $pvcMVP_{mean} = MAV \times pvcSUV_{mean}$. Finally, a global disease activity score can be generated by summing up the pvcMVPs for all FDG-avid lesions throughout the body. A review article based on the current literature related to metabolic tumor volume and total glycolysis in various solid tumors concluded that "both metabolic tumor volume and TLG have the potential to become valuable as prognostic biomarkers for survival outcome, clinical staging, and response to both neoadjuvant and concurrent therapies."[62] Therefore, we expect that the development of more sophisticated but user-friendly, automated software packages in the near future will facilitate the rapid adoption of these very important quantitative approaches. In essence, this may provide clinicians with a single number that reflect the global disease activity in many disorders at diagnosis, during therapeutic interventions and determining patient outcomes.

Dynamic Metrics (Patlak Analysis, Kinetic Models)

The availability of high-sensitivity PET scanners promoted the deployment of dynamic acquisition protocols in clinical and research settings. The acquired 4D PET data may consequently be used by graphical analysis or higher order kinetic modeling techniques to allow the derivation of quantitative maps representing physiological parameters of interest. Graphical or Patlak analysis methods initially define a set of assumptions for a compartment model and then derive simpler linearized graphical relationships models across a smaller set of parameters, also known as "macro-parameters."[63] Thus, the newly identified model equations describe a lower degree relationship between the acquired 4D PET data and the streamlined model.[14]

These developments enabled the resurgence of parametric imaging as a viable approach not only for limited FOV or single-bed imaging[64] but also in WB oncologic imaging. The main drawbacks of the former approach are that it requires prior knowledge of the body part containing the pathology to make sure that this region is adequately covered by the selected bed position. Moreover, the approach is not adequate to identify a distant disease (eg, metastasis), which is spread throughout the body. These deficiencies have been recently tackled by the proposal of a novel class of 4D WB PET imaging protocols intended for tracking the PET signal through the body, thus enabling WB imaging of macroparameters, including net uptake rate (K_i) and total blood volume distribution (V).[18] The complementary information provided by tracer uptake macroparameters might contribute in the multiparametric assessment and characterization of malignant lesions across multiple beds and in improved reproducibility in monitoring treatment response. In essence, the protocol consists in extracting the image-derived time integral of the blood input function from a 6-min dynamic scan over the heart though drawing an ROI on the left ventricle on reconstructed dynamic frames. The protocol does not restrict the initial blood pool scan, for which full compartmental modeling can be performed, to be limited over the heart region but to be chosen based on the localization of the disease within the body. This is followed by multiple scan passes, usually between six and thirteen, across multiple bed positions that are used as input to fit the Patlak model enabling to generate K_i parametric images.[14] This can be performed either post reconstruction (indirect approach) through fitting reconstructed dynamic PET images or prior to reconstruction in the project space (direct approach) through nesting the Patlak model within each tomographic update step.[65] PET data acquisition is inherently 4D spatiotemporal in nature and only implementing 4D PET imaging algorithms would enable to fully utilize the complete 4D PET dataset that has always been acquired by PET scanners.

The limited axial FOV of current generation commercial PET scanners results in the acquisition of temporally continuous dynamic PET data only for a single bed position. The direct consequence is that, contrary to the WB parametric imaging concept discussed above, full compartmental modeling is axially restricted.[14] Parametric imaging does not fully take advantage of the information that could be extracted combined with the benefits of continuous bed motion acquisition in dynamic imaging. Taking advantage of this option implemented on some recent commercial systems, a modified WB dynamic protocol was recently reported striving for providing WB Patlak analysis and full compartmental modeling in a predefined single bed FOV covering a suitable blood pool section (eg, the heart or the aorta) simultaneously.[66] In full kinetic modeling of ^{18}F-FDG, the exchanges between the compartments are modeled by the microparameters K_1 (plasma to nonphosphorylated compartment), k_2 (nonphosphorylated to plasma compartment), and k_3 (nonphosphorylated to phosphorylated compartment) rate constants. A zero efflux (dephosphorylation) rate constant ($k_4 = 0$) between the phosphorylated and the nonphosphorylated compartment is assumed. Preliminary clinical assessment of this methodology seems to suggest that parametric K_i imaging generated by full kinetic modeling ($K_i = \frac{K_1 k_3}{k_2 + k_3}$) combined with microparameters obtained for a selected single bed position brings additional value in some clinical cases. Moreover, clinically feasible dynamic WB PET imaging protocols can be implemented by modulating the bed speed within each pass based on preselected FOVs within the total WB FOV with the aim

to optimize the frame duration and counting statistics according to the a priori known location of the pathology.[27] It is expected that the advent long axial FOV total-body PET scanners will enable the implementation of fully compartmental WB parametric imaging techniques in the clinic.[67]

Radiomics Features

Radiomics is an emerging field in quantitative image analysis. The notion of radiomics is derived by combining the prefix "radio" from radiology, which refers to radiological images, for example, CT, MRI as well as PET, and the suffix "omics," which stands for the technologies that aim at providing collective and quantitative features for an entire system and explore its underlying mechanisms as in the study of genes (genomics), proteins (proteomics), and metabolites (metabolomics).[68] More formally speaking, *radiomics* is defined as the process of extraction of quantitative information from anatomical/molecular images with their corresponding biological information and clinical endpoints. Radiomics could be thought of as consisting of following two main procedures: (i) the extraction of quantitative imaging (static and dynamic features) from a previously defined tumor region(s) and (ii) the incorporation of the imaging features or traits into mathematical models for treatment outcome prediction that is aimed at providing added value for personalizing of treatment regimens in comparison with commonly used clinical predictors; this is illustrated in Figure 4.[69-71]

Although the notion of radiomics traces its origin into quantitative imaging analysis in the areas of computer-aided detection or diagnosis in the 1980s,[72] its application for clinical and biological endpoints has started in the past decade only. This has been driven by recent advances in personalized/precision medicine. It worth noting that among the early applications of radiomics has been using FDG-PET imaging for predicting radiotherapy tumor response.[73] This should not come as a surprise given the functional nature of PET and the underlying impact of intratumor metabolic heterogeneity on characterizing radiation response; an example is shown in Figure 5. This was further corroborated with series of applications of PET radiomics for predicting response in cancers of the esophagus,[74] head and neck,[75] and lung cancer,[76] among others. Moreover, the combination of PET/CT was shown to predict local control in nonsmall cell lung cancer,[77] while the combination of PET/MRI was shown to improve prediction of metastasis to the lung in sarcoma.[77] Reviews of these applications are provided in the works of Constanzo et al. and Avanzo et al.[71,78]

The features extracted from PET images (radiomics) could be derived via direct extraction (handcrafted) or indirectly using deep learning methodology. The latter is still in its infancy and we will focus in this review on the direct feature extraction methods, which has witnessed tremendous growth and success over the past decade. Direct radiomic features can be divided into static (time invariant) and dynamic (time varying) features according to the acquisition protocol at the time of scanning and into pre- or intra-treatment features according to the scanning time point. Examples of static and dynamic features used in the literature are described in the following and summarized in the Table from the work of El Naqa.[79]

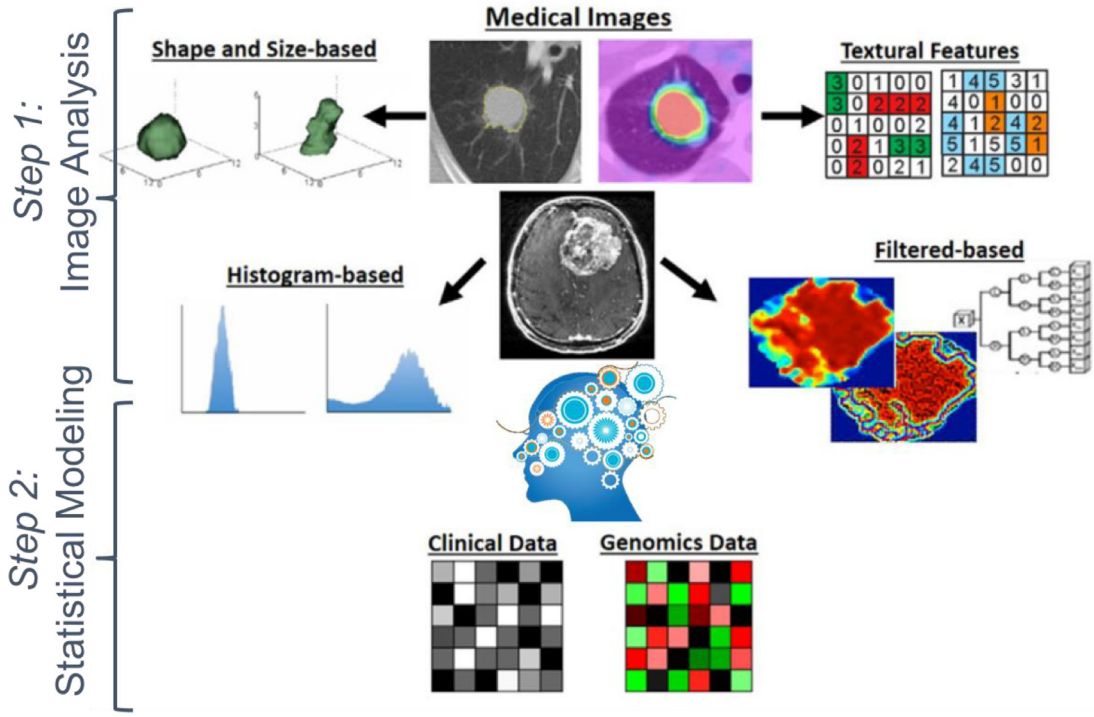

Figure 4 Schematic of radiomics workflow showing the two main steps of feature extraction and model building involved. Adapted from Yip and Aerts.[102]

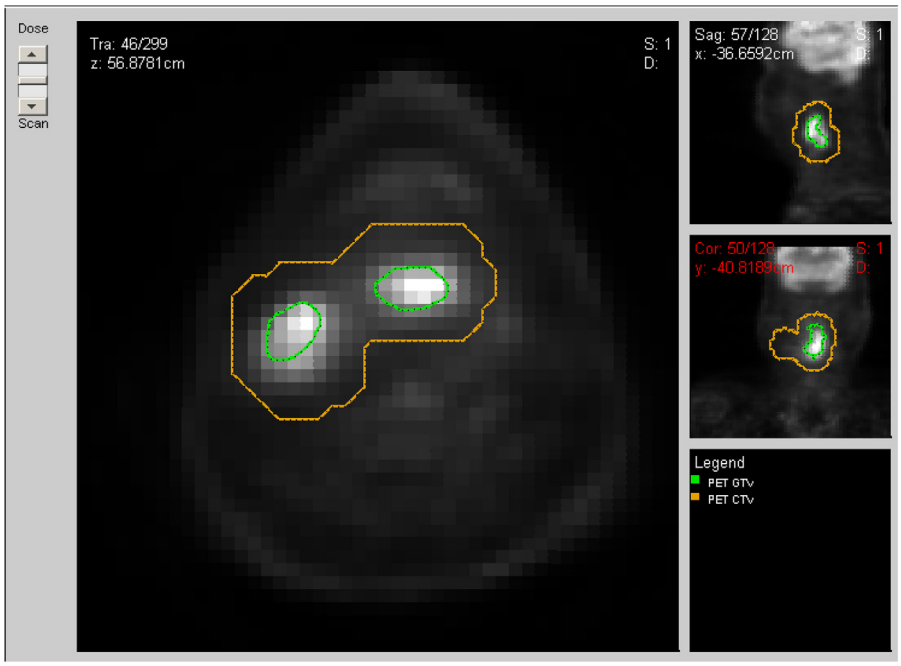

(A)

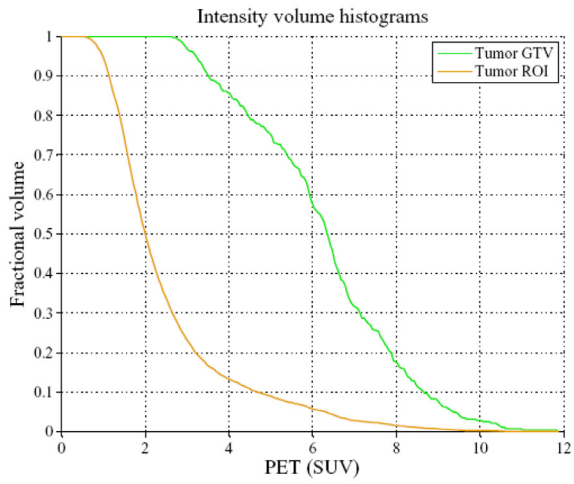

(B)

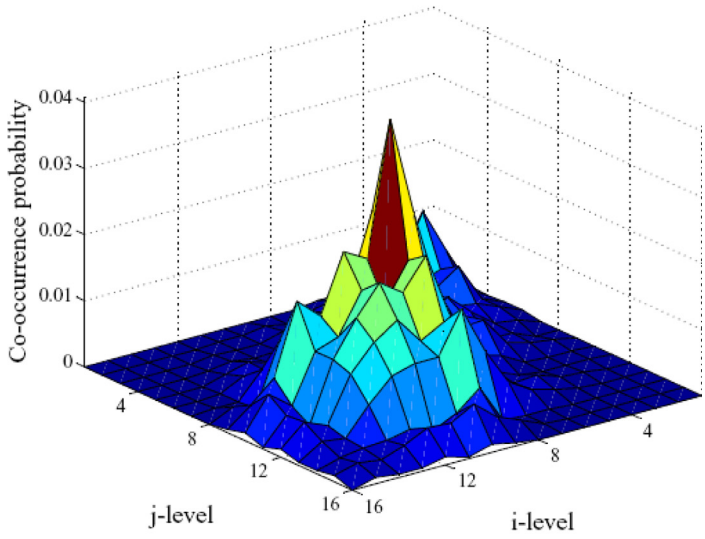

(C)

Figure 5 (A) A pretreatment PET scan of a head-and-neck cancer case of patient who died from disease after radiotherapy treatment. The head and neck tumor ROI (brown) and the gross-tumor volume (green) were outlined by the physician. (B) An IVH plot, where I_x and V_x parameters are derived. (C) A texture map plot of the gross-tumor volume heterogeneity through intensity-spatial mapping.

Static/Dynamic Features (IVH, Shape, Texture, etc)

Intensity—volume histogram (IVH): This is analogous to the use of dose volume histogram applied in radiotherapy treatment planning for reducing complicated 3D data into a single easier to interpret curve. Each point on the IVH curve defines the absolute or relative volume of the structure (tumor or normal tissue) that exceeds the intensity in relative or absolute sense,[73] see Figure 5B. The IVH approach would allow for extracting several metrics from PET images for outcome analysis such as I_x (minimum intensity to x% highest intensity volume), V_x (percentage volume having at least x% intensity value), in addition to descriptive statistics (mean, minimum, maximum, standard deviation, etc).

Morphologic (shape) features: These are generally geometrical shape attributes such as eccentricity (a measure of nonsphericity), which can describe tumor progression direction, Euler number (the number of connected objects in a region excluding the number of holes), which is useful for describing lesions with necrotic regions, and solidity (a measurement of convexity), which may be characteristic of benign vs malignant lesions.[80,81] An interesting demonstration of this

Table Summary of commonly extracted radiomics variables from PET images for outcome modeling in oncology.

Category	Example features	Comments
SUV global descriptive measurements	Maximum	The highest single value within an ROI. Sometimes corrected for body mass index.
	Peak	Derived from a circular ROI of 0.75 to 1.5 cm in diameter centered on the maximum-value pixel and evaluate the mean SUV within this ROI;
	Total lesion glycolysis	$SUV_{mean} \times$ tumor volume
	Other statistics	Mean, minimum, standard deviation, coefficient of variation, skewness, kurtosis
IVH metrics	V_x (5-100 in steps of 5 as percentage of the SUV uptake)	Percentage volume receiving x% intensity
	I_x (5-100 in steps of 5)	Minimum intensity to x% volume
	Heterogeneity metrics	Differences of I_x and V_x measures
Texture-based features	Gray level co-occurrence matrix	Second-order histogram features (energy, entropy, contrast, and homogeneity, etc)
	Neighborhood gray tone difference matrix	Higher order histogram features (coarseness, contrast, busyness, and complexity)
	Run-length matrix	Regional run-length features
	Gray level size-zone matrix	Regional zone features
	Fractals	Self-similar patterns (fractal dimensions)
	Other metrics	Law energy features, Gabor filter, SIFT, etc
Shape-based features	Eccentricity Euler Number Solidity Extent	Geometric and topological characteristics
Kinetic parameters	Compartmental/graphical modeling parameters	Parameters extracted from dynamic PET imaging (eg, FDG-kinetics)

principle has been shown in sarcoma using an idealized ellipsoid structure (ie, eccentricity), which was indicative of metastatic behavior.[81,82]

Texture features: Imaging texture is a second-order histogram and refers to the relative distribution of intensity values within a given neighborhood. Texture integrates intensity with spatial information resulting in a local neighborhood. Textures are generally independent of tumor position, orientation, size, and brightness, and can take into account the local intensity-spatial distribution.[83,84] Texture methods are broadly divided into following three categories: statistical methods (eg, high-order statistics, co-occurrence matrices, and moment invariants), model-based methods (eg, Markov random fields, Gabor filters, and wavelet transforms), and structural methods (eg, topological descriptors and fractals).[85,86] Among these methods, statistical approaches based on the co-occurrence matrix and its variants such as the gray level co-occurrence matrix (Fig. 5C), neighborhood gray tone difference matrix, run-length matrix, and gray level size-zone matrix have been widely applied for characterizing PET uptake heterogeneity.[87]

Dynamic features: These features are based on the analysis of kinetic maps extracted from tissue compartment models as discussed above. Image features (such as IVH, texture, and morphology) can be derived from these kinetic maps.

Modeling Approaches (Regression Models, Machine Learning (Shallow/Deep))

In the context of radiomics analysis, the observed clinical endpoints are considered to be a function of derived imaging metrics. Before radiomics modeling with explicit features, a selection process is required to identify the best subset of features. There are principally three types of techniques existing for such feature selection task, namely, filter methods, wrapper methods, and embedded methods. The filter-based method is an information-theoretical method, which is simple and computationally efficient (eg, mutual information, cross-correlations, and relief). Wrapper methods utilize the targeted classifier's prediction performance to rank the features. The embedded method implements the feature selection into the process of the classifier training. Deep learning further bypasses this process by abstracting the data representation as part of the training of the algorithm, assuming enough data or procedures such as data augmentation/transfer learning can be applied.[88] With the optimized chosen feature, a radiomics model can be built such as classical logistic regression approaches or more advanced ML techniques. For more details about outcome modeling in oncology, the readers can refer to the textbook by El Naqa.[89] We will provide some examples using regression and ML techniques in the following.

Radiomics Modeling by Logistic Regression

Logistic regression is a common tool for statistical model learning. It involves a logit transformation, which is given by

$$f(\mathbf{x}_i) = \frac{e^{g(\mathbf{x}_i)}}{1 + e^{g(\mathbf{x}_i)}}, \quad i = 1, \ldots n, \tag{1}$$

where n is the number of samples, $\mathbf{x}_i$ is a vector of the radiomics features used to predict $f(\mathbf{x}_i)$ for outcome y_i (clinical or biological endpoints) of the ith

$$g(\mathbf{x}_i) = \beta_o + \sum_{j=1}^{d} \beta_j x_{ij}, i = 1, \ldots, n, j = 1, \ldots, d, \tag{2}$$

where d is the number of radiomics features and the β's are model coefficients determined by maximum likelihood techniques. The number of parameters can be determined using standard search methods or by utilizing regularization approaches, such as LASSO.

Radiomics Modeling by Machine Learning

ML represents an important class of artificial intelligence algorithms (eg, neural networks, decision trees, random forests, support vector machines (SVMs), and deep learning neural networks), which are able to learn complex patterns from the labeled (supervised) or unlabeled (unsupervised) data.[90] SVMs and neural networks are among the most commonly used ML methods in radiomics. Given a data with inputs x_i, and labels y_i, $D = \{(\boldsymbol{x_i}, \boldsymbol{y_i}) \in R^n \times C \mid i = 1, 2, 3, \ldots, N\}$ of N total samples, a function f: $R^n \rightarrow C$ can be estimated. Following two types of problems can be addressed: *classification*, when the target set C is discrete, or *regression*, when C is continuous. In the case of classification, for example, discriminating low vs high risk cases of tumor failure, SVM develops a hyperplane that can separate the different class categories as follows:

$$Max_{\boldsymbol{w},b,r} r$$

with

$\|\boldsymbol{w}\| = 1$ and $(\langle \boldsymbol{w}, \boldsymbol{x_i} \rangle + b) \cdot \boldsymbol{y_i} \geq r, \quad i = 1, 2, \ldots, N$, where $r \in \boldsymbol{R}$, $\boldsymbol{w} \in \boldsymbol{R^n}, b \in \boldsymbol{R}$, and $\boldsymbol{y_i} = \{\boldsymbol{1}, \boldsymbol{-1}\}$. The optimal weights $(\boldsymbol{w}, \boldsymbol{b})$ determine the SVM classifier:

$$f_{SVM}(\boldsymbol{x}) = g(\langle \boldsymbol{w}, \boldsymbol{x} \rangle + b), \tag{3}$$

where g is an indicator function.

On the other hand, neural networks construct a nonlinear mapping using a recursive weighting procedure $\{\mathbf{W}^{(l)} = W_{jk}^{(l)} \mid l = 1, 2, 3, \ldots\}$ and vectors (bias) $\{\boldsymbol{b}^{(l)} = b_m^{(l)} \mid l = 1, 2, 3, \ldots\}$ such that

$$f_{NN}(\boldsymbol{x}) = \cdots \sigma\left(\mathbf{W}^{(2)} \cdot \sigma\left(\mathbf{W}^{(1)} \cdot \boldsymbol{x} + \boldsymbol{b}^{(1)}\right) + \boldsymbol{b}^{(2)}\right), \tag{4}$$

where σ: $R^p \rightarrow R^q$ is a nonlinear function known as the *activation function*. The index $l = 1, 2, 3, \ldots$ indicates the network depth, which is called *layers*. A network is referred to as shallow if it had a small number of layers (<3), otherwise, it is referred to as a deep network.

Deep neural network has recently shown remarkable performance in a variety of biomedical problems, such as patient's risk of cancer, diagnosis, and prognosis of treatment response.[91] Deep neural networks do not require explicit extraction of features as discussed above and can learn the embedded data representation during the training process, assuming sufficient information for training data is available via data augmentation of transfer learning.

Example Application of Radiomics in Clinical Decision Support

Prediction of Survival Using Pretreatment FDG-PET

In a co-operative study, Ohri et al. presented radiomics model from 201 patients using the LASSO logistic regression model.[92] They identified a textural feature (SumMean from the gray-level co-occurrence matrix) as an independent predictor of overall survival. The feature complemented volume (MTV) in a decision tree model as shown in Figure 6. A more general approach based on random forest using PET/CT was applied for predicting clinical endpoints in head-and-neck cancer, as shown in Figure 7.[93]

Association of Radiomics With Biological Endpoints (Radiogenomics)

The process of linking radiomics features to biological endpoints is an emerging field known as radiogenomics, not to be confused with using genetics for predicting radiotherapy response. This field provides tremendous opportunities to interrogate underlying molecular biology at the macroscopic level, that is, *image-based (radiomics) biopsies*. This has been shown using CT imaging for predicting EGFR mutations in lung cancer[94-96] and in the case of PET imaging, where Yip et al. showed that 29 radiomic features can significantly predict EGFR status,[97] whereas Minamimoto et al. further showed that inverse coefficient of variation (1/COV) was a predictive factor of EGFR mutations status, independent of metabolic tumor diameter.

Comparative Effectiveness (Different Treatment Modalities (Combined Therapies, X-ray vs Particle, etc))

Proton therapy enjoys a constrained exit dose compared to standard photon treatments due to the presence of the so-called Bragg peak. This in addition to its other radiobiological advantages makes an attractive option for radiotherapy treatments. However, uncertainties associated with the location of the Bragg peak can create high risks of missing the target or causing unnecessary toxicities. PET imaging has emerged as a useful tool for range verification in proton therapy, which can measure the β+ activity induced by beam-tissue interactions during treatment.[98] An example using the INSIDE (Innovative

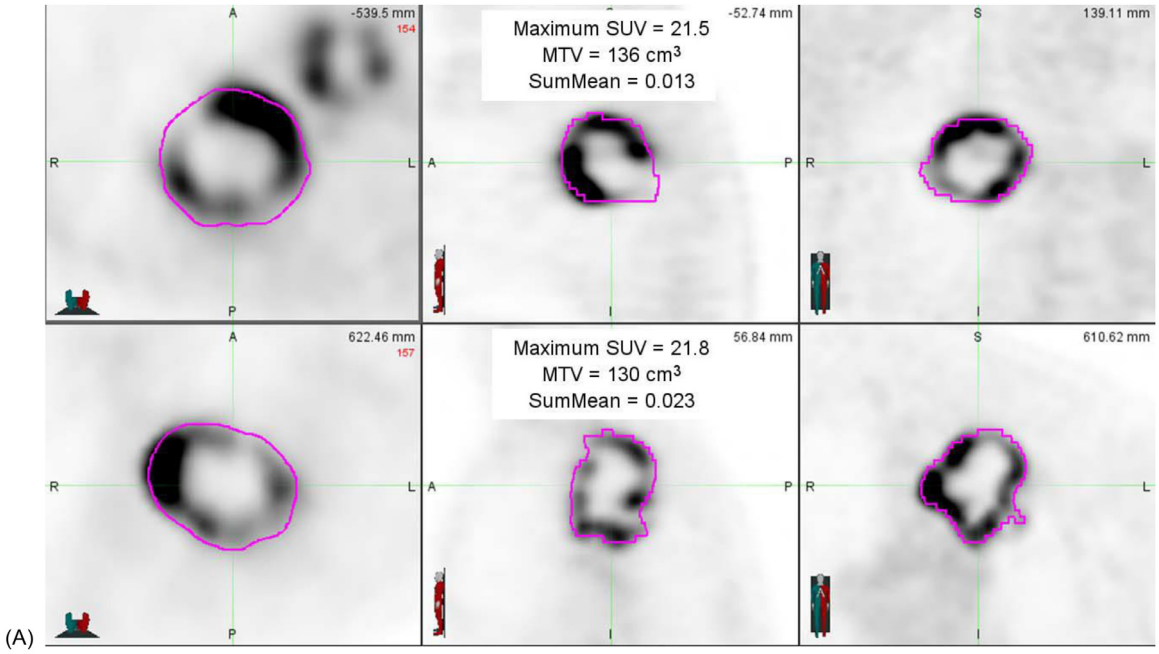

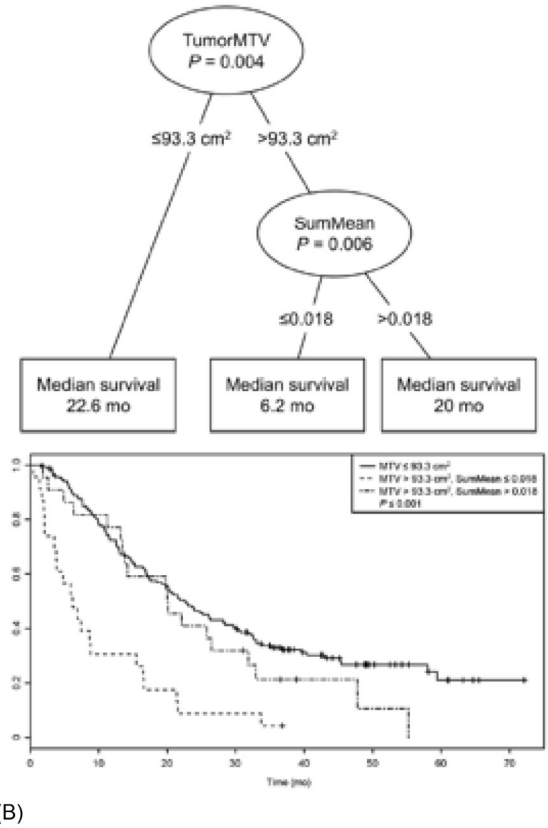

Figure 6 Modeling of patients' survival using PET imaging. (A) PET images from two sample patients whose tumors had similar metabolic tumor volume and SUV_{max} and similar appearances but disparate SumMean values. Both tumors were scored as markedly heterogeneous based on visual examination. Survival time for the patient in the upper panel was 15.5 months, compared with 47.8 months for the patient in the lower panel. (B) Conditional inference tree for the combination of metabolic tumor volume and SumMean as predictors of overall survival (top), and corresponding Kaplan–Meier curves for overall survival for the three groups resulting from the tree-defined cutpoints (bottom).

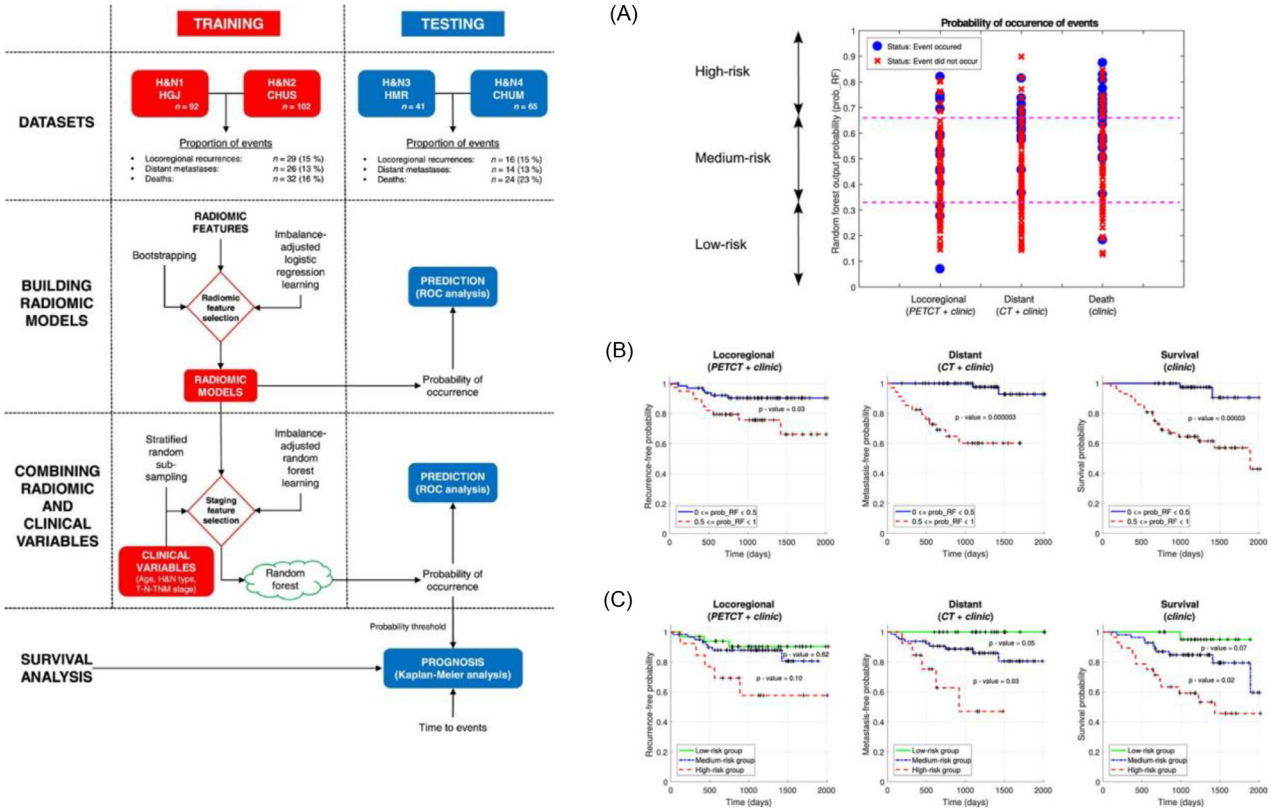

Figure 7 Radiomics prediction by ML (random forest) application. (Left) Models construction strategy and analysis workflow. Four different cohorts were used to demonstrate the utility of radiomics analysis for the pretreatment assessment of the risk of locoregional recurrence and distant metastases in head-and-neck cancer. The H&N1 and H&N2 cohorts were combined and used as a single training set ($n = 194$), whereas the H&N3 and H&N4 cohorts were combined and used as a single testing set ($n = 106$). The best combinations of radiomic features were selected in the training set using imbalance-adjusted logistic regression learning and bootstrapping validations. These radiomic features were combined with selected clinical variables in the training set using imbalance-adjusted random forest learning and stratified random subsampling validations. Independent prediction analysis was performed in the testing set for all classifiers fully constructed in the training set. Independent prognosis analysis and Kaplan–Meier risk stratification were carried out in the testing set using the output probability of occurrence of events of random forests fully constructed in the training set. (Right) Risk assessment of tumor outcomes in Vallieres et al.[93] (A) Probability of occurrence of events for each patient of the testing set. The output probability of occurrence of events of random forests allows for risk stratification. (B) Kaplan–Meier curves of the testing set using a risk stratification into two groups as defined by a random forest output probability threshold of 0.5. All curves show significant prognostic performance. (C) Kaplan–Meier curves of the testing set using a risk stratification into three groups as defined by random forest output probability thresholds of 1/3 and 2/3.

Solutions for In-beam DosimEtry in hadrontherapy) is shown in Figure 8.[99] The INSIDE in-beam PET scanner features two planar heads of $10 \times 25\,cm^2$ active area, each made of 2×5 detection modules with 16×16 Lutetium Fine Silicate crystals coupled to Hamamatsu MPPCs, resulting in 2560^2 LORs. The system was able to achieve a range agreement of about 1 mm.

Adaptive Therapy and Dose Escalation Studies

PET imaging, and in particular FDG-PET, has been used for dose escalation studies in radiotherapy. In a recent study of lung cancer, an adaptive RT-escalated dose based on FDG-avid region detected by midtreatment positron PET was shown to improve local tumor control at 2-y follow-up.[100] However, dose adaptation in such a study is based on clinician's subjective assessment. Alternatively, to objectively assess the adaptive dose per fraction, a three-component deep reinforcement learning (DRL) approach with neural network architecture was developed. The DRL was trained on large-scale patient characteristics including clinical, genetic, and imaging radiomics features in addition to tumor and lung dosimetric variables. In comparison with the clinical protocol,[100] the DRL achieved a root mean-squared error (RMSE) = 0.5 Gy for dose escalation recommendation. Interestingly, the DRL seemed to suggest better decisions than the clinical ones in terms of mitigating toxicity risks and improving local control, as shown in Figure 9.[101] This demonstrates the potential power of the combination radiomics with ML

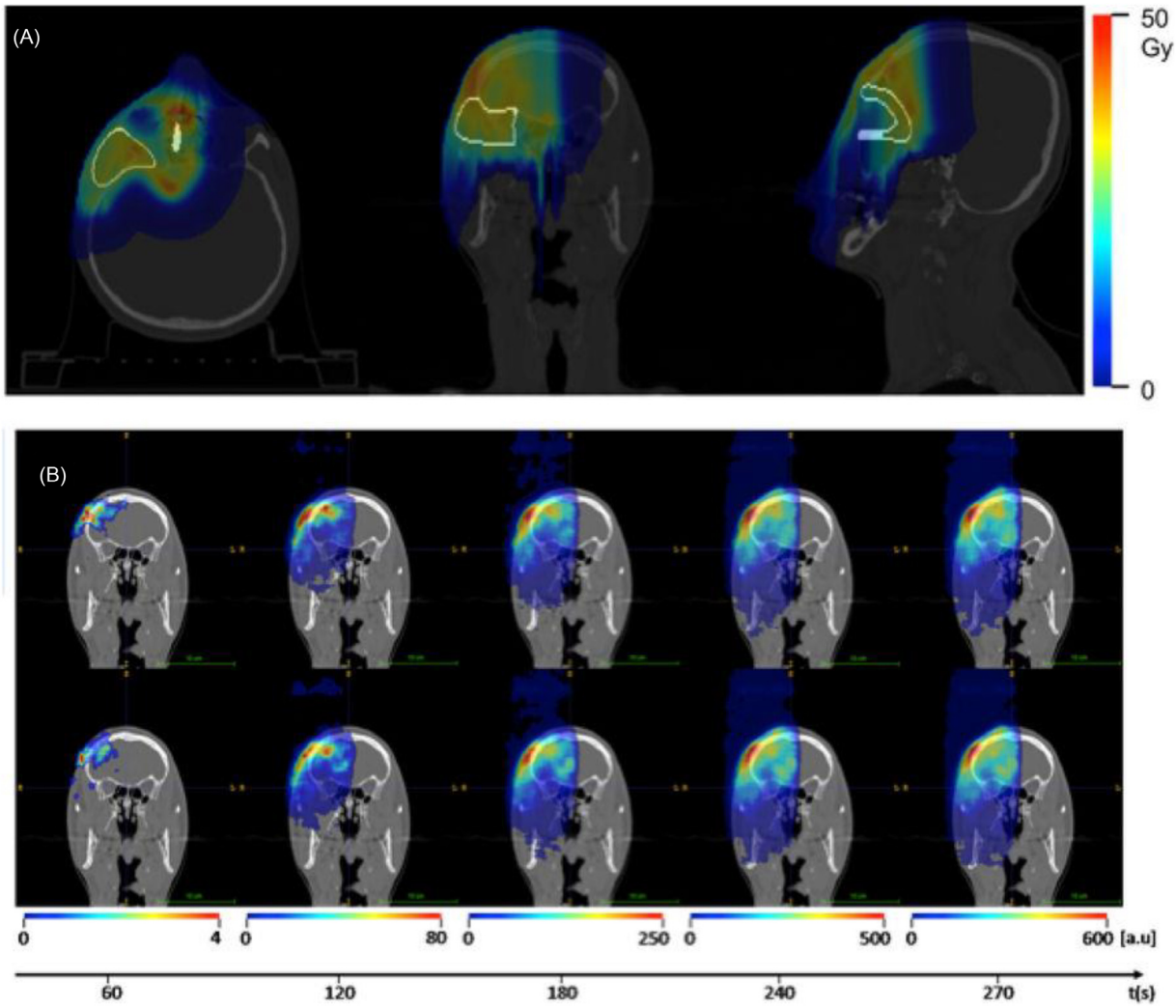

Figure 8 An example for online proton monitoring using PET. Treatment plan and set up. (A) Axial (left), coronal (center), and sagittal (right) sections of the patient CT with the planned dose distribution to be delivered in the beam field monitored with the INSIDE in-beam PET system and the clinical target volume superimposed in white. (B) Time evolution of a 2D slice of the detected beam-induced activity superimposed to the patient's CT used for dose planning. The top and bottom rows refer to the first (December 1, 2016) and second (December 2, 2016) acquisition days, respectively.

for such applications; however, further validation studies are still needed.

Concluding Remarks and Future Directions

PET is commonly utilized for the in vivo assessment of a large array of specific malignancy mechanisms, depending on the employed radiotracer, thereby offering high specificity. Despite the challenges faced, quantitative PET imaging including radiomics may be associated with high clinical potential in oncology. Major advancements have been achieved during the last decade with the deployment of quantitative imaging biomarkers involving the use of either conventional static imaging and semi-quantitative indices or parametric imaging based on full kinetic analysis using spatiotemporal image reconstruction, which is expected to enter the clinical arena during the next few years and replace commonly used analytical techniques.

This is undoubtedly an exciting time for quantitative imaging in clinical oncology. It is gratifying to see in an overview the tremendous progress that quantitative imaging has made, from straightforward semi-quantitative analysis to texture heterogeneity analysis methods and radiomics, and most recently towards WB parametric imaging combined with full kinetic modeling for a limited axial FOV containing the pathology. During the last few decades, the number of papers reporting on the development or use of advanced quantitative imaging methodologies supporting their clinical has been growing steadily. There is no scarcity of challenges and opportunities for quantitative molecular imaging techniques at the present time. There is still scope for ground-breaking methodological developments in the field, and given the imagination and creativity of talented researchers, the future of quantitative imaging is definitely bright.

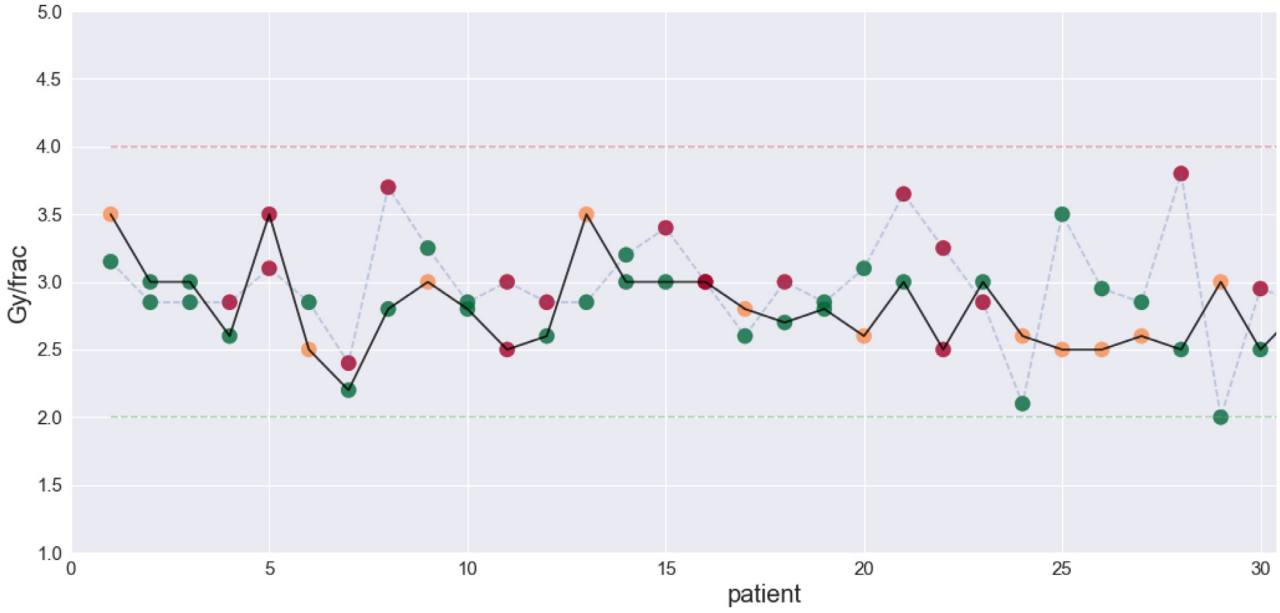

Figure 9 A deep RL for automated radiation adaptation in lung cancer. DQN (black solid line) vs clinical decision (blue dashed line) with RMSE error = 0.5 Gy. An evaluation against eventual outcomes of good (green dots), bad (red dots), and potentially good decisions (orange dots) is shown, suggesting not only comparable but also instances of better overall performance by the DQN. Reprinted with permission from Tseng et al.[101]

Acknowledgements

This work was supported by the Swiss National Science Foundation under Grant SNSF 320030_176052 and the Swiss Cancer Research Foundation under Grant KFS-3855-02-2016.

References

1. Zaidi H, Alavi A: Trends in PET quantification: Opportunities and challenges. Clin Transl Imaging 2:183-185, 2014
2. Pimlott SL, Sutherland A: Molecular tracers for the PET and SPECT imaging of disease. Chem Soc Rev 40:149-162, 2011
3. Valliant JF: A bridge not too far: Linking disciplines through molecular imaging probes. J Nucl Med 51:1258-1268, 2010
4. de Jong M: New tracers to the clinic. Q J Nucl Med Mol Imaging 61:133-134, 2017
5. Mach RH: New targets for the development of PET tracers for imaging neurodegeneration in Alzheimer disease. J Nucl Med 55:1221-1224, 2014
6. Zaidi H (ed): Quantitative Analysis in Nuclear Medicine Imaging. New York: Springer, 2006
7. Basu S, Zaidi H, Houseni M: Novel quantitative techniques for assessing regional and global function and structure based on modern imaging modalities: Implications for normal variation, aging and diseased states. Sem Nucl Med 37:223-239, 2007
8. Weber WA, Schwaiger M, Avril N: Quantitative assessment of tumor metabolism using FDG-PET imaging. Nucl Med Biol 27:683-687, 2000
9. Acton PD, Zhuang H, Alavi A: Quantification in PET. Radiol Clin N Am 42:1055-1062, 2004
10. Houshmand S, Salavati A, Hess S: An update on novel quantitative techniques in the context of evolving whole-body PET imaging. PET Clinics 10:45-58, 2015
11. Boellaard R: Need for standardization of 18F-FDG PET/CT for treatment response assessments. J Nucl Med 52(suppl 2):93-100, 2011
12. Bai B, Bading J, Conti PS: Tumor quantification in clinical positron emission tomography. Theranostics 3:787-801, 2013
13. van der Vos CS, Koopman D, Rijnsdorp S: Quantification, improvement, and harmonization of small lesion detection with state-of-the-art PET. Eur J Nucl Med Mol Imaging 44:4-16, 2017
14. Zaidi H, Karakatsanis N: Towards enhanced PET quantification in clinical oncology. Br J Radiol 91:20170508, 2018
15. Zhou J, Qi J: Efficient fully 3D list-mode TOF PET image reconstruction using a factorized system matrix with an image domain resolution model. Phys Med Biol 59:541-559, 2014
16. Huang SC: Anatomy of SUV. Standardized uptake value. Nucl Med Biol 27:643-646, 2000
17. Bentourkia M, Zaidi H: Tracer kinetic modeling in PET. PET Clinics 2:267-277, 2007
18. Karakatsanis NA, Lodge MA, Tahari AK: Dynamic whole-body PET parametric imaging: I. Concept, acquisition protocol optimization and clinical application. Phys Med Biol 58:7391-7418, 2013
19. Rahmim A, Tang J, Zaidi H: Four-dimensional (4D) image reconstruction strategies in dynamic PET: Beyond conventional independent frame reconstruction. Med Phys 36:3654-3670, 2009
20. Reader AJ, Verhaeghe J: 4D image reconstruction for emission tomography. Phys Med Biol 59:R371-R418, 2014
21. Kotasidis F, Matthews J, Reader A: Direct Parametric Reconstruction for Dynamic 18F-FDG PET/CT Imaging in the Body. In: In: Proceedings of the IEEE Nuclear Science Symposium and Medical Imaging Conference (NSS/MIC):Anahaim, CA,USA3383-3386, 2012
22. Frank R: Quantitative Imaging Biomarkers Alliance FDG-PET/CT Working Group report. Mol Imaging Biol 10:305, 2008
23. Clarke LP, Nordstrom RJ, Zhang H: The quantitative imaging network: NCI's historical perspective and planned goals. Translational Oncology 7:1-4, 2014
24. Conti M: Focus on time-of-flight PET: The benefits of improved time resolution. Eur J Nucl Med Mol Imaging 38:1147-1157, 2011
25. Zhou WV, Kyme AZ, Meikle SR: A scheme for PET data normalization in event-based motion correction. Phys Med Biol 54:5321-5339, 2009
26. Panin VY, Smith AM, Hu J: Continuous bed motion on clinical scanner: Design, data correction, and reconstruction. Phys Med Biol 59:6153-6174, 2014
27. Kotasidis FA, Garibotto V, Zaidi H: Patient-Specific Hybrid Whole-Body PET Parametric Imaging from Speed Modulated Continuous Bed

Motion Dynamic Data. In: Proceedings of the IEEE Nuclear Science Symposium and Medical Imaging Conference (NSS/MIC); 2017
28. Reader AJ, Zaidi H: Advances in PET image reconstruction. PET Clinics 2:173-190, 2007
29. Abdoli M, Dierckx RA, Zaidi H: Metal artifact reduction strategies for improved attenuation correction in hybrid PET/CT imaging. Med Phys 39:3343-3360, 2012
30. Ahmadian A, Ay MR, Bidgoli JH: Correction of oral contrast artifacts in CT-based attenuation correction of PET images using an automated segmentation algorithm. Eur J Nucl Med Mol Imaging 35:1812-1823, 2008
31. Mehranian A, Arabi H, Zaidi H: Vision 20/20: Magnetic resonance imaging-guided attenuation correction in PET/MRI: Challenges, solutions, and opportunities. Med Phys 43:1130-1155, 2016
32. Srinivas SM, Dhurairaj T, Basu S: A recovery coefficient method for partial volume correction of PET images. Ann Nucl Med 23:341-348, 2009
33. Surti S, Karp JS: Imaging characteristics of a 3-dimensional GSO whole-body PET camera. J Nucl Med 45:1040-1049, 2004
34. Rousset O, Rahmim A, Alavi A: Partial volume correction strategies in PET. PET Clin 2:149-235, 2007
35. Torigian DA, Lopez RF, Alapati S: Feasibility and performance of novel software to quantify metabolically active volumes and 3D partial volume corrected SUV and metabolic volumetric products of spinal bone marrow metastases on (18)F-FDG-PET/CT. Hell J Nucl Med 14:8-14, 2011
36. Hickeson M, Yun M, Matthies A: Use of a corrected standardized uptake value based on the lesion size on CT permits accurate characterization of lung nodules on FDG-PET. Eur J Nucl Med Mol Imaging 29:1639-1647, 2002
37. Avril N, Bense S, Ziegler SI: Breast imaging with fluorine-18-FDG PET: Quantitative image analysis. J Nucl Med 38:1186-1191, 1997
38. Zaidi H, Montandon M-L, Assal F: Structure-function based quantitative brain image analysis. PET Clin 5:155-168, 2010
39. Bundschuh R, Martínez-Möller A, Essler M: Local motion correction for lung tumours in PET/CT—First results. Eur J Nucl Med Mol Imaging 35:1188-1981, 2008
40. Nehmeh SA: Respiratory motion correction strategies in thoracic PET-CT imaging. PET Clin 8:29-36, 2013
41. Wahl RL, Jacene H, Kasamon Y: From RECIST to PERCIST: Evolving considerations for PET response criteria in solid tumors. J Nucl Med 50(suppl 1):122-150, 2009
42. Zasadny KR, Wahl RL: Standardized uptake values of normal tissues at PET with 2-[fluorine-18]-fluoro-2-deoxy-D-glucose: Variations with body weight and a method for correction. Radiology 189:847-850, 1993
43. Kim CK, Gupta NC, Chandramouli B: Standardized uptake values of FDG: body surface area correction is preferable to body weight correction. J Nucl Med 35:164-167, 1994
44. Weber WA, Ziegler SI, Thodtmann R: Reproducibility of metabolic measurements in malignant tumors using FDG PET. J Nucl Med 40:1771-1777, 1999
45. Pierce LA 2nd, Elston BF, Clunie DA: A digital reference object to analyze calculation accuracy of PET standardized uptake value. Radiology 277:538-545, 2015
46. Zaidi H, El Naqa I: PET-guided delineation of radiation therapy treatment volumes: A survey of image segmentation techniques. Eur J Nucl Med Mol Imaging 37:2165-2187, 2010
47. Hatt M, Lee J, Schmidtlein CR, El Naqa I: Classification and evaluation strategies of auto-segmentation approaches for PET: Report of AAPM Task Group No. 211. Med Phys 44:e1-e42, 2017
48. Berthon B, Spezi E, Galavis P: Towards a standard for the evaluation of PET auto-segmentation methods: Requirements and implementation. Med Phys 44:4098-4111, 2017
49. Hatt M, Laurent B, Ouahabi A: The first MICCAI challenge on PET tumor segmentation. Med Image Anal 44:177-195, 2018
50. Alavi A, Newberg AB, Souder E: Quantitative analysis of PET and MRI data in normal aging and Alzheimer's disease: Strophy weighted total brain metabolism and absolute whole brain metabolism as reliable discriminators. J Nucl Med 34:1681-1687, 1993
51. Larson SM, Erdi Y, Akhurst T: Tumor treatment response based on visual and quantitative changes in global tumor glycolysis using PET-FDG imaging. The visual response score and the change in total lesion glycolysis. Clin Positron Imaging 2:159-171, 1999
52. Basu S, Saboury B, Torigian D: Current evidence base of FDG-PET/CT imaging in the clinical management of malignant pleural mesothelioma: Emerging significance of image segmentation and global disease assessment. Mol Imaging Biol 13:801-811, 2011
53. Berkowitz A, Basu S, Srinivas S: Determination of whole-body metabolic burden as a quantitative measure of disease activity in lymphoma: A novel approach with fluorodeoxyglucose-PET. Nucl Med Commun 29:521-526, 2008
54. Basu S, Saboury B, Werner T: Clinical utility of FDG-PET and PET/CT in non-malignant thoracic disorders. Mol Imaging Biol 13:1051-1060, 2011
55. Saboury B, Salavati A, Brothers A: FDG PET/CT in Crohn's disease: Correlation of quantitative FDG PET/CT parameters with clinical and endoscopic surrogate markers of disease activity. Eur J Nucl Med Mol Imaging 41:605-614, 2014
56. Abdulla S, Salavati A, Saboury B: Quantitative assessment of global lung inflammation following radiation therapy using FDG PET/CT: A pilot study. Eur J Nucl Med Mol Imaging 41:350-356, 2014
57. Saboury B, Parsons MA, Moghbel M: Quantification of aging effects upon global knee inflammation by 18F-FDG-PET. Nucl Med Commun 37:254-258, 2016
58. Jonnakuti VS, Raynor WY, Taratuta E: A novel method to assess subchondral bone formation using [18F]NaF-PET in the evaluation of knee degeneration. Nucl Med Commun 39:451-456, 2018
59. Bural GG, Torigian DA, Chamroonrat W: Quantitative assessment of the atherosclerotic burden of the aorta by combined FDG-PET and CT image analysis: A new concept. Nucl Med Biol 33:1037-1043, 2006
60. Beheshti M, Saboury B, Mehta NN: Detection and global quantification of cardiovascular molecular calcification by fluoro18-fluoride positron emission tomography/computed tomography-a novel concept. Hell J Nucl Med 14:114-120, 2011
61. Mehta NN, Torigian DA, Gelfand JM: Quantification of atherosclerotic plaque activity and vascular inflammation using [18-F] fluorodeoxyglucose positron emission tomography/computed tomography (FDG-PET/CT). J Vis Exp 2:e3777, 2012
62. Van de Wiele C, Kruse V, Smeets P: Predictive and prognostic value of metabolic tumour volume and total lesion glycolysis in solid tumours. Eur J Nucl Med Mol Imaging 40:290-301, 2013
63. Patlak CS, Blasberg RG: Graphical evaluation of blood-to-brain transfer constants from multiple-time uptake data. Generalizations. J Cereb Blood Flow Metab. 5:584-590, 1985
64. Dimitrakopoulou-Strauss A, Strauss LG, Heichel T: The role of quantitative (18)F-FDG PET studies for the differentiation of malignant and benign bone lesions. J Nucl Med 43:510-518, 2002
65. Karakatsanis NA, Casey ME, Lodge MA, Rahmim A, Zaidi H: Whole-body direct 4D parametric PET imaging employing nested generalized Patlak expectation-maximization reconstruction. Phys Med Biol 61:5456-5485, 2016
66. Kotasidis FA, Garibotto V, Zaidi H: Hybrid Whole-Body Dynamic TOF PET Imaging for Simultaneous Estimation of Compartmental and Patlak Parametric Maps from Continuous Bed Motion Data. In: Proceeding of the IEEE Nuclear Science Symposium and Medical Imaging Conference (NSS/MIC); 2016
67. Cherry SR, Jones T, Karp JS: Total-body PET: Maximizing sensitivity to create new opportunities for clinical research and patient care. J Nucl Med 59:3-12, 2018
68. Gillies RJ, Kinahan PE, Hricak H: Radiomics: Images are more than pictures, they are data. Radiology 278:563-577, 2016
69. Kumar V, Gu Y, Basu S: Radiomics: The process and the challenges. Magn Reson Imaging 30:1234-1248, 2012
70. Gillies RJ, Anderson AR, Gatenby RA: The biology underlying molecular imaging in oncology: From genome to anatome and back again. Clin Radiol 65:517-521, 2010

71. Constanzo J, Wei L, Tseng HH: Radiomics in precision medicine for lung cancer. Transl Lung Cancer Res 6:635-647, 2017
72. Doi K: Computer-aided diagnosis in medical imaging: Historical review, current status and future potential. Comput Med Imaging Graph 31:198-211, 2007
73. El Naqa I, Grigsby P, Apte A: Exploring feature-based approaches in PET images for predicting cancer treatment outcomes. Pattern Recognit 42:1162-1171, 2009
74. Tixier F, Le Rest CC HattM: Intratumor heterogeneity characterized by textural features on baseline 18F-FDG PET images predicts response to concomitant radiochemotherapy in esophageal cancer. J Nucl Med 52:369-378, 2011
75. Cheng N-M, Dean Fang Y-H, Tung-Chieh Chang J: Textural features of pretreatment 18F-FDG PET/CT images: Prognostic significance in patients with advanced T-stage oropharyngeal squamous cell carcinoma. J Nucl Med 54:1703-1709, 2013
76. Cook GJR, Yip C, Siddique M: Are pretreatment 18F-FDG PET tumor textural features in non-small cell lung cancer associated with response and survival after chemoradiotherapy? J Nucl Med 54:19-26, 2013
77. Vaidya M, Creach KM, Frye J: Combined PET/CT image characteristics for radiotherapy tumor response in lung cancer. Radiother Oncol 102:239-245, 2012
78. Avanzo M, Stancanello J, El Naqa I: Beyond imaging: The promise of radiomics. Phys Med 38:122-139, 2017
79. El Naqa I: The role of quantitative PET in predicting cancer treatment outcomes. Clin Transl Imaging 2:305-320, 2014
80. Jain AK: Fundamentals of Digital Image Processing. Englewood Cliffs, NJ: Prentice Hall, 1989
81. O'Sullivan F, Roy S, O'Sullivan J: Incorporation of tumor shape into an assessment of spatial heterogeneity for human sarcomas imaged with FDG-PET. Biostat 6:293-301, 2005
82. O'Sullivan F, Roy S, Eary J: A statistical measure of tissue heterogeneity with application to 3D PET sarcoma data. Biostat 4:433-448, 2003
83. Castleman KR: Digital Image Processing. Englewood Cliffs, NJ: Prentice Hall, 1996
84. Haralick R, Shanmugam K, Dinstein I: Texture features for image classification. IEEE Trans Syst Man Cybern 3:610-621, 1973
85. Zhang J, Tan T: Brief review of invariant texture analysis methods. Pattern Recognit 35:735-747, 2002
86. Castellano G, Bonilha L, Li LM: Texture analysis of medical images. Clin Radiol 59:1061-1069, 2004
87. Chicklore S, Goh V, Siddique M: Quantifying tumour heterogeneity in 18F-FDG PET/CT imaging by texture analysis. Eur J Nucl Med Mol Imaging 40:133-140, 2013
88. Goodfellow I, Bengio Y, Courville A: Deep Learning. Cambridge, MA: The MIT Press, 2016
89. El Naqa I: A Guide to Outcome Modeling In Radiotherapy and Oncology: Listening to the Data ed. Boca Raton, FL: CRC Press: Taylor & Francis, 2018
90. El Naqa I, Li R, Murphy MJ: Machine Learning in Radiation Oncology: Theory and Application eds. Switzerland: Springer International Publishing, 2015
91. LeCun Y, Bengio Y, Hinton G: Deep learning. Nature 521:436, 2015
92. Ohri N, Duan F, Snyder BS: Pretreatment 18F-FDG PET textural features in locally advanced non-small cell lung cancer: Secondary analysis of ACRIN 6668/RTOG 0235. J Nucl Med 57:842-848, 2016
93. Vallieres M, Kay-Rivest E, Perrin LJ: Radiomics strategies for risk assessment of tumour failure in head-and-neck cancer. Sci Rep 7:10117, 2017
94. Aerts HJWL, Grossmann P, Tan Y: Defining a radiomic response phenotype: A pilot study using targeted therapy in NSCLC. Sci Rep 6:33860, 2016
95. Gevaert O, Echegaray S, Khuong A: Predictive radiogenomics modeling of EGFR mutation status in lung cancer. Sci Rep 7:41674, 2017
96. Liu Y, Kim J, Balagurunathan Y, Li Q: Radiomic features are associated with EGFR mutation status in lung adenocarcinomas. Clin Lung Cancer 17:441-448.e6, 2016
97. Yip SSF, Parmar C, Kim J: Impact of experimental design on PET radiomics in predicting somatic mutation status. Eur J Radiol 97:8-15, 2017
98. Paganetti H, El Fakhri G: Monitoring proton therapy with PET. Br J Radiol 88:20150173, 2015
99. Ferrero V, Fiorina E, Morrocchi M: Online proton therapy monitoring: Clinical test of a silicon-photodetector-based in-beam PET. Sci Rep 8:4100, 2018
100. Kong F, Ten Haken RK, Schipper M: Effect of midtreatment PET/CT-adapted radiation therapy with concurrent chemotherapy in patients with locally advanced non-small-cell lung cancer: A phase 2 clinical trial. JAMA Oncol 3:1358-1365, 2017
101. Tseng HH, Luo Y, Cui S: Deep reinforcement learning for automated radiation adaptation in lung cancer. Med Phys 44:6690-6705, 2017
102. Yip SS, Aerts HJ: Applications and limitations of radiomics. Phys Med Biol 61:R150-R166, 2016